Streamlined Behavioural Modelling of GaN HEMTs for Pulsed-Power Applications

Ivan Vorotiahin, *Member, IEEE*, Martin Hergt, Martin Sack, *Member, IEEE*, Marc Hiller, *Member, IEEE*, and Georg Müller, *Member, IEEE*

***Abstract*—A streamlined method to model GaN high electron mobility transistor's (HEMT) behaviour based on I-V measurements is proposed in this article. A model based on Angelov's model is used to this end, modified to account for the device's off-tail of the transconductance function and the steeper output conductance behaviour in the ohmic regime, as well as the effects of self-heating. The resulting model features an equation for the equivalent circuit's current source with its numerical parameters obtained from the step-wise fitting of the measurement data. The fitting helps with modelling the current-voltage dependency of a GaN HEMT in the cases when the input dataset provides insufficient number of operating points to assess all critical parameters of the Angelov model using standard techniques.**

***Index Terms*—Gallium nitride, High electron mobility transistor, Simulation, Pulsed measurements.**

I. Introduction

With the widening field of applications for the pulsed-power devices [1], arises the need for switches that can achieve shorter rise times while providing similar output currents and voltages as the state-of-the-art SiC MOSFET-based switches [2]. While the rise-time of tens of nanoseconds is achieved in the contemporary semiconductor-based pulsed-power switches, and the single-digit-nanosecond rise time is achievable when SiC MOSFETs are gate-boosted [3]–[5], there is an entire type of GaN-based high electron mobility transistors capable of achieving even faster switching [6], [7] thanks to their structure using a 2D layer with highly mobile charge carriers as a conductive channel [8].

GaN HEMTs are relatively new on the market and their development is still ongoing [8]. This creates a need to characterize the emerging devices and create their models that can be used to predict the behaviour under the typical operating conditions, when built into pulsed-power circuits – i.e., focusing on short pulses, time resolutions down to hundreds of picoseconds, as well as output voltages of hundreds of volts [9]. While the technological processes have learned to deal with some of the physical effects negatively affecting GaN HEMT's operation, such as surface-trapping induced gate lag [10], [11], they are still affected by the buffer-layer trapping and self-heating [12], [13]. The effect of the former manifests as drain lag and takes milli- to microseconds to influence the output current's behaviour. The self-heating, on the other hand, is known to impact the efficiency of GaN HEMTs, especially in high-power applications [14]. Enabling the device's model to account for the self-heating and differenciate it from other effects, such as channel length modulation, provides advantages for the simulation quality [15].

The methods and tools commonly used to simulate GaN HEMTs' behaviour branch from the models for GaAs MESFETs [16]–[19]. Decades of the gathered knowledge have resulted in the wide variety of physical and behavioural models, primarily used in the power and high-frequency electronics circuit designs [20]–[22], and algorithms to capture and represent the aforementioned dispersive effects [14], [23], [24]. In the scope of our interest is the family of behavioural models proposed and elaborated by Angelov *et al.* in 1992 [18], [25]. It describes the HEMT's characteristics using parameters that can be obtained from the pulsed measurements, and presents a circuit of parasitic components that can be calculated from the measured S-parameters. With the development of the GaN HEMT technology, there is a constant need to refine various aspects of the modelling [26], [27] to describe emerging devices in the operating regimes dictated by their usage. Although contemporary GaN HEMTs often come with manufacturer-provided models, that can serve as important references, characteristics obtained via simulations with them (*e.g.*, S-parameters) demonstrate deviations from the measurements [28] and due to their black-box nature cannot be improved to address them nor expanded to take into account further dispersive effects.

A method to characterize modern types of power electronics devices, including GaN HEMTs, has been proposed in [29], [30] which uses pulsed S-parameter measurements to provide both S-parameters and I-V dependencies for output drain voltages up to 40 V in the ON-state and up to 500 V in the OFF-state. Using S-parameters as an input, the iterative optimisation algorithm [28], [30]–[32], computes the values of the parasitic components in the measured range based on the equivalent circuit equations. This article expands the work by providing a streamlined method to simulate a nonlinear current source with a modification of the Angelov model, using current-voltage characteristics that can be measured with the same or a similar experimental setup as described in [29], [30] and taking into account the limitations in the density of measured data points when wide range of operating parameters have to be characterized.

Manuscript received December 00, 2024; revised Month 00, 2025.

Ivan Vorotiahin, Martin Sack, and Georg Müller are with the Institute for Pulsed Power and Microwave Technology (IHM), Karlsruhe Institute of Technology, 76131 Karlsruhe, Germany (e-mail: ivan.vorotiahin@kit.edu)

Martin Hergt is with the Siemens AG Technology, Erlangen, Germany

Marc Hiller is with the Institute of Electrical Engineering (ETI), Karlsruhe Institute of Technology, 76131 Karlsruhe, Germany

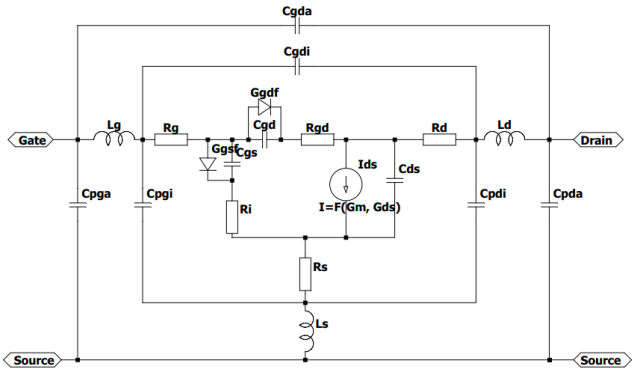

Fig. 1. Small-signal equivalent circuit of a GaN HEMT as used in [28].

II. The Model

The chosen model represents a GaN HEMT as a non-linear current source surrounded by an equivalent circuit of parasitic components, as exemplarily shown in Figure 1. The current source is described by a bias-dependent function, parameters for which can be found by analyzing current-voltage characteristics obtainable from pulsed measurements [13], [33]. The values for external and bias-dependent intrinsic components of the equivalent circuit can be found numerically from the S-parameter measurements and are specific for each considered operating point [31]. The transconductance G_m and output conductance R_{ds} in the small-signal operation regime represent the linearized behaviour of the transistor. In the large-signal regime, they are both included into the equation for the voltage controlled current source I_{ds} as parameters denoting its dependence on the gate U_{gs} and drain U_{ds} bias voltages respectively. The classical equation for the current source is given in [25] as

$$I_{ds}(U_{gs},U_{ds}) = I_{pk}(U_{ds})\cdot(1+\tanh(\Psi(U_{gs},U_{ds}))) \cdot\tanh(\alpha_1(U_{gs})U_{ds})\cdot(1+\lambda(U_{gs})U_{ds}), \quad (1)$$

where I_{pk} is the current, at which transconductance G_m reaches its maximum value; α_1 is a saturation behaviour parameter dependent on the output conductivity G_{ds} near $U_{ds}=0$, λ is a parameter of channel modulation describing an increment of the output current in saturation regime, and Ψ is a series of the form [25]:

$$\Psi(U_{gs},U_{ds}) = \frac{1}{I_{pk}(U_{ds})}(G_m|_{U_{gs}=U_{pk}(U_{ds})})\cdot(U_{gs}-U_{pk}(U_{ds})) + \frac{\partial G_m}{\partial U_{gs}}|_{U_{gs}=U_{pk}(U_{ds})}\cdot(U_{gs}-U_{pk}(U_{ds}))^2 + \frac{\partial^2 G_m}{\partial U_{gs}^2}|_{U_{gs}=U_{pk}(U_{ds})}\cdot(U_{gs}-U_{pk}(U_{ds}))^3+...), \quad (2)$$

featuring derivatives of the output current by the gate bias taken at U_{pk}, which is gate voltage at which G_m reaches its maximum value.

While in the saturation regime, U_{pk} and I_{pk} are constant, they become dependent on the drain bias U_{ds} in the ohmic regime [25].

To account for thermal effects, due to device's self-heating during the operation, Equation (1) has to be supplemented with a thermal term turning it into

$$I_{ds}^{\theta} = I_{ds}\cdot(1-\Theta P_{diss}) \quad (3)$$

representing the decrease of the saturation current due to heat dissipation P_{diss} [34]. Θ in this equation is a parameter denoting heat storage and release, usually represented with a thermal RC-sub-circuit [35]. The thermal part of Equation (3) depends not only on the gate and drain bias, but also on the device temperature θ, which can be represented indirectly [15] via environment temperature θ_e. Their interrelationship can be described with the expression [15]:

$$\theta = \theta_e + Z_\theta P_{diss}, \quad (4)$$

where $Z_\theta(\theta_e)$ is thermal impedance.

To develop a simulation strategy and test its applicability for the evaluation of the available measurement data, the Angelov model was applied to the current-voltage characteristics of a market-available GaN HEMT [36]. One set of data has been generated from its simulation using a model provided by the Manufacturer to gradually improve the algorithm by increasing the complexity of the input. The second characterization comes from the pulsed measurements described in [28], taken during the S-parameter characterization and featuring self-heating effects.

A. Modifications of the Model

As a starting point of the model implementation, the idealized I-V characteristics of the transistor Maufacturer's model was recreated using Equation (1) with its parameters found using their definitions from [25]. Figure 2 illustrates the consecutive steps taken to eliminate discrepancies between the original I-V characteristics and the recreated ones.

The first implementation of the original equation, shown with blue curves in Figure 2, highlights an important issue with the original Angelov model described, *e.g.*, in [27]. Equation (1) operates under the assumption of a bell-shaped form of transconductivity G_m, which in the real contemporary devices tend to have a significant "tail" gradually falling towards higher U_{gs} [27], which – in turn – leads to significant underestimation of the output current (see Fig. 3a). As a solution, we propose to supplement Equation (1) with a coefficient dependent on U_{gs} while retaining and scaling its behaviour in the Ohmic regime. The new coefficient I_{pk}^{tail} would take values of the saturation current I_S in the saturation regime and is defined as

$$I_{pk}^{tail}(U_{gs},U_{ds}) = \frac{I_{pk}(U_{ds})I_S(U_{gs})}{I_{pkS}}, \quad (5)$$

where I_{pkS} is I_{pk} in the saturation regime. The implementation of this coefficient is shown in Figure 2 with red curves.

The second point of improvement adresses the underestimation of the currents in the ohmic operating regime. A closer look to the output conductance (see Figure 3b) of the characterized model shows that it has a non-linear behaviour near zero that can be emulated by adding a quadratic term of

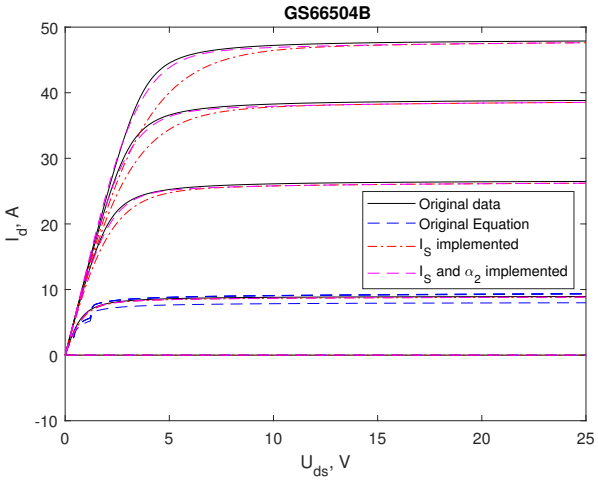

Fig. 2. Stages of Angelov model's implementation to recreate the idealized characteristics of a contemporary GaN HEMT [36]. Black curves show the data from the manufacturer's model. Blue curve represents the result after the implementation of Equation (1) directly. Red curves represent the result after using the saturation current value to better represent the "tail" of G_m. Purple curves represent the result after expanding the saturation behaviour part of the equation with a quadratic term.

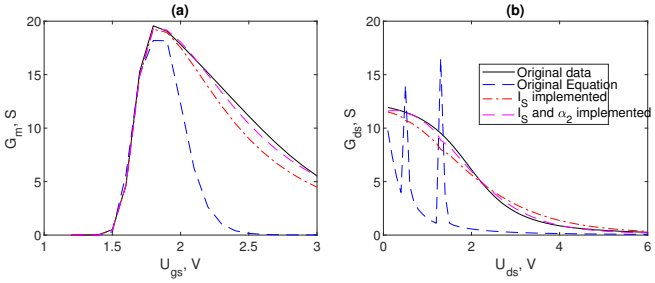

Fig. 3. Transconductance (a) and output conductance (b) of a modelled transistor described by the Angelov model using the original equation (blue dashed curve), after accounting for the transconductance tail (red dash-dotted curve) and after expanding the saturation behaviour term (purple dashed curve) compared to the original data (black solid curve).

U_{ds} into the saturation behaviour term under the hyperbolic tangent, so that the final equation would have the following shape:

$$I_{ds}(U_{gs},U_{ds}) = I_{pk}^{tail}(U_{gs},U_{ds}) \cdot (1+\tanh(\Psi(U_{gs},U_{ds}))) \cdot \tanh(\alpha_1(U_{gs})U_{ds} + \alpha_2(U_{gs})U_{ds}^2) \cdot (1+\lambda(U_{gs})U_{ds}), \quad (6)$$

where α_2 is a coefficient dependent on the $\frac{\partial G_{ds}}{\partial U_{ds}}$ and can be estimated via fitting. The resulting I_{ds} after the implementation of this equation is shown as the purple curves in Figure 2.

B. Direct Fitting

Equation 6 provides us with a model describing the voltage-dependent current source of a GaN HEMT. This formula needs at least 7 bias-dependent parameters, receivable via analysis of measured output current curves. The process of finding all necessary values for the equation can be simplified by using numerical software. By rewriting bias-dependent parameters in the whole expression into a set of functions, it is possible to fit the whole measured I-V characteristics, as a surface dependent on U_{gs} and U_{ds}, to Equation 6. Several values derived from the measurements can be stated as initial values for the fitting process. MATLAB Fitting Toolbox [37] was used to search for the fit function and its parameters. The expressions for I_{pk}^{tail}, Ψ, α_1, α_2, λ have been initially taken from their definitions in [25] and iteratively modified, together with the initial values, until the minimum of mean-square error has been achieved, shown in Figure 4. The corresponding expressions are:

$$I_{pk}^{tail} = I_{pkS}\exp(S_1U_{gs})\exp(S_2U_{ds}), \quad (7)$$

$$\alpha_1 = \alpha_{1c}\tanh(A_{10}+A_{11}U_{gs}), \quad (8)$$

$$\alpha_2 = \alpha_{2c}\tanh(A_{20}+A_{21}U_{gs}), \quad (9)$$

$$\lambda = \lambda_c\tanh(\Lambda U_{gs}), \quad (10)$$

$$\Psi = P_1\left(1+\left(\frac{1}{\cosh(BU_{ds})}\right)^2\right)\cdot(U_{gs}-U_{pk}) + P_2\exp(CU_{ds})\cdot(U_{gs}-U_{pk})^2 + P_3\cdot(U_{gs}-U_{pk})^3, \quad (11)$$

where the initial value of I_{pkS} is I_{pk} in saturation area, P_1 starting value is $G_{m,pkS}/I_{pkS}$ (maximum transconductivity over the correspondent current in the saturation area), α_{1c} starting value is derived from the output conductance near zero drain bias and gate bias U_{pk} as $G_{ds,pk0}/I_{pkS}$, while S_1, S_2, P_2, P_3, α_{2c}, A_{10}, A_{11}, A_{20}, A_{21}, λ_c, and Λ are fitting coefficients introduce to emulate the bias dependence of the parameters. Based on the form of the U_{pk} dependence on the drain bias obtained from the I-V curve analysis in the ohmic and active regimes, it can be approximated to the hyperbolic tangential

$$U_{pk}(U_{ds}) = \frac{U_{pkS}-U_{pk0}}{2}\left(\tanh\left(\frac{U_{ds}}{U_S}-\frac{U_S}{2}\right)+1\right)+U_{pk0}, \quad (12)$$

where U_S is the saturation drain voltage at U_{pk}, U_{pkS} and U_{pk0} are U_{pk} measured in the saturation regime and at U_{ds} close to zero, respectively.

C. Thermal Effects

After establishing an algorithm for simulating the GaN HEMT based on its intrinsic characteristics, an important step is to estimate the changes in its behaviour that would come up when the thermal effects stop being negligible. Equation (3) describes transistor's self-heating and represents it as a drop in the output current. Already knowing values of the Angelov equation from the previous step, we can fit the I-V curves taken for different ambient temperatures θ_e to establish not only bias-, but also temperature dependence of the equation parameters Θ and P_{diss}. This iteration of direct fitting uses already established numerical values for the isothermal part of the equation (Equation (6)) and fits both thermal parameters. The best fit, corresponding to the minimum of the mean-square error, represents the thermal parameters in the following form:

$$\Theta = \Theta_0\exp(\Theta_1U_{gs}+\Theta_2), \quad (13)$$

$$P_{diss} = p_0\cdot(\tanh(p_{01}U_{gs}+p_{02})\tanh(p_{03}U_{ds}+p_{04})) + p_1\cdot(\tanh(p_{11}U_{gs}+p_{12})\tanh(p_{13}U_{ds}+p_{14})), \quad (14)$$

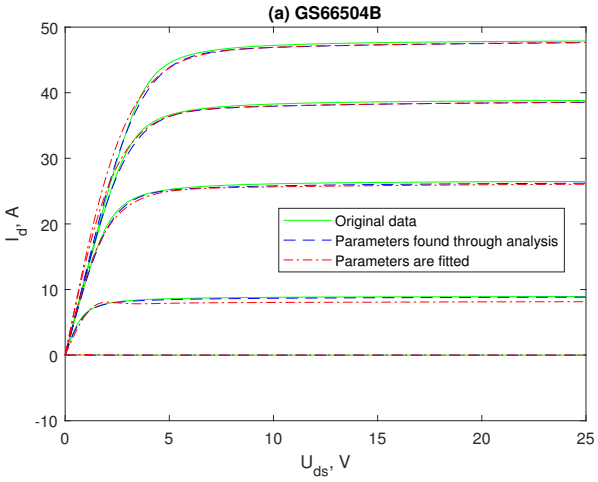

Fig. 4. Comparison of the I_{ds} characteristics shown for the gate biases from 1 to 5 V. Green lines represent the simulation data using the manufacturer's model; blue dashed curves represent its simulation using the Angelov model, parameters for which were found from original curves analysis; red dot-dashed curves represent the simulation using the Angelov model with parameters found via direct fitting.

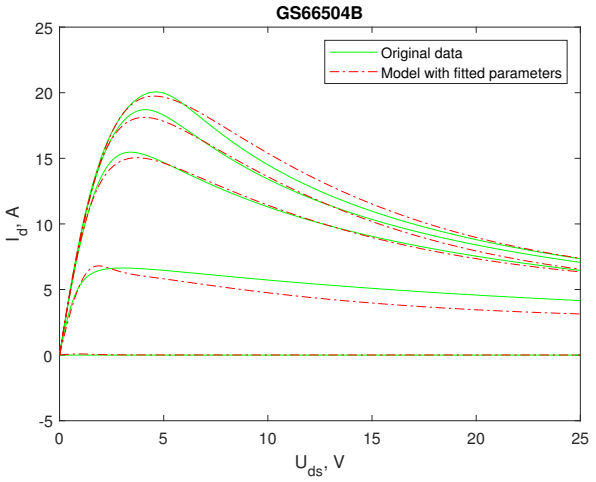

Fig. 5. Comparison of the I_{ds} characteristics shown for the gate bias between 1 and 5 V accounting for the self-heating, at the external temperature $\theta_e = 25$°C. Green lines represent the simulation data using the manufacturer's model; red dot-dashed curves represent the simulation using the Angelov model with parameters found via direct fitting.

with Θ_n and p_n being fitting parameters dependent on temperature, introduced to account for the bias dependence of Θ and P_{diss}. Using external temperature as a parameter, we performed fitting for the external temperature range of $\theta_e = 0...50$°C, which allows us to represent their dependence in the form of

$$Z(\theta_e) = Z_0 + Z_1\Delta\theta_e + Z_2(\Delta\theta_e)^2, \tag{15}$$

with Z representing each of the fitting parameters and Z_0 its value at $\theta_e = 0$°C. The quadratic term can be left out, if a coefficient can be well characterized with a linear temperature dependence. Additionally, Equation (14) can be used with just the first term, if there is not much measured information about power dissipation, but a need to keep the number of fitting coefficients low. Data from the characterization of a real device [28] includes the distribution of P_{diss} that can be well fitted with Equation (14), as will be shown in the next section. Figure 5 shows an example of the I-V curves for the GaN HEMT model with thermal effects.

III. Validation

To test the described algorithm on the real measurements, characterization data from [28] has been used as an input. The most important constraints, represented by this dataset, that this algorithm tries to address are the following:

1) All measurements exhibit some influence of the device's self-heating due to the measurement process with slow pulses [28], [30];
2) The measured operating points are sparse between ohmic and saturation regimes, which may impede finding of some of the Angelov equation parameters.

The first constraint is the most important one, since without clear distinction between the isothermic and temperature-dependent parts of the equation, the fitting coefficients may drift further away from their physically sound values. While θ_e is constant, the device temperature now depends on the operation time t: P_{diss} in Equation (4) is time-dependent. At the same time, to account for thermal impulse response in time domain [34], we include it into the fitting coefficient Θ, making it time-dependent. The measured data contains device temperatures calculated from the corresponding P_{diss} [28]. Thus, we can use t as a parameter in the termal part of the I^{θ}_{ds} equation. The time-dependence of the fitting coefficients in Equations (13) and (14) can also be described by the expression used for the ambient temperature dependence in Equation (15), substituting $\Delta\Theta_e$ with Δt. In this case, Z_0 corresponds to the coefficient value at the first fitted time point. It is worth noting that no consistent similarities has been found between θ_e- and t-dependencies of the same P_{diss} and Θ coefficients.

With no further information apart from the output current measurements, it is still possible to fit the measurement data to the temperature-dependent fonction I^{θ}_{ds} from Equation (3) and then, while keeping the coefficients for the isothermal part constant, to fit the thermal part to data for different stages of self-heating. However, the available measurement data also contains information about P_{diss} over bias and operation time ranges. Thus, in this case, the computational sequence consists of three following steps:

1) Obtaining parameters for P_{diss} by fitting its distribution to Equation (14) for the whole range of the operation times t;
2) Choosing one fixed time point and using the corresponding P_{diss} values, obtain the rest of the I^{θ}_{ds} parameters, including Θ;
3) Perform the fitting of the I^{θ}_{ds} for Θ parameters over the operation time range, with fixed temperature-independent parameters, found in the previous step, and using P_{diss} values for the respective t.

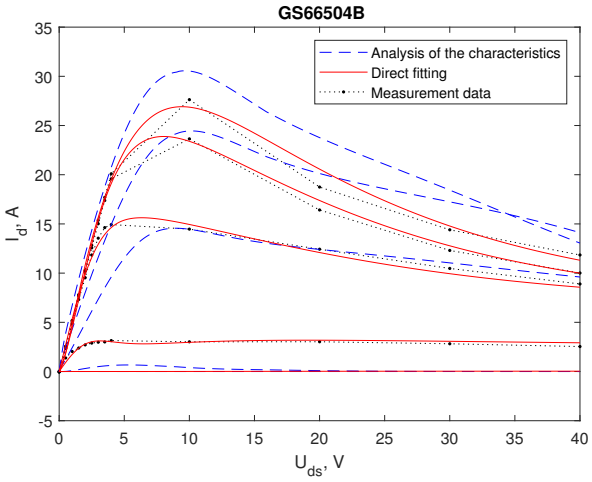

Fig. 6. Comparison of the I_{ds} characteristics shown for the gate bias U_{gs} from 1 to 5 V. Black dots represent the measured data; blue dashed curves represent the simulation using the Angelov model, parameters for which were found from measurement curve analysis; red curves represent the simulation using the Angelov model with parameters found via direct fitting.

TABLE I
PARAMETERS OF THE I_{ds} EQUATION, SHOWN FOR $t = 464$ µs

I_{pkS}	S_1	S_2
7.64	0.198	–0.0033
U_{pkS}	U_{pk0}	U_S
2.64	2.37	2.3
P_1	P_2	P_3
0.556	–1.25	0.297
α_{1c}	A_{10}	A_{11}
87.2	$6.18 \cdot 10^{-3}$	$-8.9 \cdot 10^{-4}$
λ_c	Λ	
$-4.04 \cdot 10^{-5}$	–1.46	
B	C	
$3.16 \cdot 10^{-5}$	–0.141	
Θ_0	Θ_1	Θ_2
3.28	–0.112	0.966
p_0	p_{01}	p_{02}
0.208	0.44	–0.637
p_{03}	p_{04}	
0.0346	0.0358	
p_1	p_{11}	p_{12}
–0.0312	2.02	–2.94
p_{13}	p_{14}	
0.041	0.209	

Figure 6 displays the measured I_{ds}^{theta} of the characterized GaN HEMT and its simulations with the Angelov model. The blue curves represent the Angelov model with its parameters found by the standard means of analysis and characterization. The red curves were obtained via direct fitting. The coefficients for the I_{ds}^{θ} equation found to obtain this characteristics are listed in Table I. The obvious downside of the direct fitting path is that the fitting coefficients drift further away from their realistic values the more iterations it takes to fit the current-voltage characteristics to a 3D surface. However, when it comes to the output current values, it provides more accurate replication than the traditional parameter characterization method, represented by the blue curves.

One further difference worth noting is that when fitted directly, the output current equation does not require the quadratic drain-bias term with α_2 parameter. This is most likely because the bias-dependence of the parts of the expression for Ψ, given in Equation (2) as derivatives of the transconductance G_m, could be found easier via direct fitting.

IV. Discussion and Conclusions

We have illustrated the case, when the sparseness of the measured data complicates the determination of the parameters, necessary to formulate the Angelov model, such as the maximum transconductivity along with the associated values of current and voltage. The simulation process involving direct fitting of the Angelov's equation for the non-linear current source to the measured data was shown to be advantageous, as it can be used to simulate a GaN HEMT under such constraints. This is helpful in case if the characterization measurements are time-consuming. For example, the data for the output current analyzed here was obtained as a part of the S-parameters characterization. During the measurements, 300-microsecond long pulses were applied to the device, with slow, 50-µs-long pulse rise, to avoid oscillations and effect of drain-lag on the measurment results [28], [30]. This made the significant self-heating in the saturation region unavoidable. In this case, the data on heat dissipation was helpful to significantly improve the simulation results.

The trade-off of physically realistic model parameters for the number of datapoints is something to be considered when planning characterization measurements of GaN HEMTs. The characterization of a device for the usage in pulsed-power applications potentially implies measuring it in a broad range of bias voltages whith a reduced density of datapoints – which is where the proposed method has the advantages. It can be refined and improved to describe more operation ranges, such as reversed operation regime, and account for dispersive effects, such as drain lag and variable threshold voltage.

Acknowledgments

This research was funded by the German Research Foundation (DFG) grant No. 462921712, in the framework of the Priority Programme SPP 2312 "GaNius" (DFG project No. 441885089).

References

[1] S. Xiao, *Pulsed Power Generators*. Singapore: Springer Singapore, 2021, pp. 339–372. [Online]. Available: https://doi.org/10.1007/978-981-10-5113-5_15

[2] J. van Oorschot, "Flexible, solid-state, nanosecond pulsed power for plasma activated water generation," Doctoral thesis, Eindhoven University of Technology, Eindhoven, the Netherlands, 2023.

[3] M. Sack, S. Keipert, M. Hochberg, M. Greule, and G. Mueller, "Design considerations for a fast stacked-MOSFET switch," *IEEE Transactions on Plasma Science*, vol. 41, no. 10, pp. 2630–2636, 2013.

[4] M. Sack, M. Hochberg, D. Herzog, and G. Mueller, "Fast SiC-MOSFET switch with gate boosting technology," in *PCIM Europe digital days 2021; International Exhibition and Conference for Power Electronics, Intelligent Motion, Renewable Energy and Energy Management*, 2021, pp. 1–7.

[5] T. Okuda and T. Hikihara, "High-speed gate driver using GaN HEMTs for 20-MHz hard switching of SiC MOSFETs," 2017. [Online]. Available: https://arxiv.org/abs/1711.02832

[6] M. Sack, D. Herzog, M. Hochberg, G. Müller, G. Loisch, and F. Obier, "A solid state pulse generator for driving kicker magnets," in *2023 PulPoKS-Workshop (Pulse Power for Kicker Systems)*, 2023, 38.05.01; LK 01.

[7] M. Sack, D. Herzog, and G. Müller, "Blumlein-generator with a GaN-HEMT in gate-boosted operation as closing switch," in *2024 IEEE International Power Modulator and High Voltage Conference (IPMHVC)*, 2024.

[8] A. A. Fletcher and D. Nirmal, "A survey of gallium nitride HEMT for RF and high power applications," *Superlattices and Microstructures*, vol. 109, pp. 519–537, 2017. [Online]. Available: https://www.sciencedirect.com/science/article/pii/S0749603617312120

[9] M. Paraliev, "Development of GaN HEMT based positive/negative, 5 kV, nanosecond pulse generator for the SLS 2.0 fast injection kicker," in *2022 IEEE International Power Modulator and High Voltage Conference (IPMHVC)*, 2022, pp. 49–52.

[10] S. Binari, K. Ikossi, J. Roussos, W. Kruppa, D. Park, H. Dietrich, D. Koleske, A. Wickenden, and R. Henry, "Trapping effects and microwave power performance in AlGaN/GaN HEMTs," *IEEE Transactions on Electron Devices*, vol. 48, no. 3, pp. 465–471, 2001.

[11] M. Meneghini, A. Tajalli, P. Moens, A. Banerjee, E. Zanoni, and G. Meneghesso, "Trapping phenomena and degradation mechanisms in GaN-based power HEMTs," *Materials Science in Semiconductor Processing*, vol. 78, pp. 118–126, 2018, wide band gap semiconductors technology for next generation of energy efficient power electronics. [Online]. Available: https://www.sciencedirect.com/science/article/pii/S1369800117321716

[12] D. Bisi, M. Meneghini, M. Van Hove, D. Marcon, S. Stoffels, T.-L. Wu, S. Decoutere, G. Meneghesso, and E. Zanoni, "Trapping mechanisms in GaN-based MIS-HEMTs grown on silicon substrate," *physica status solidi (a)*, vol. 212, no. 5, pp. 1122–1129, 2015. [Online]. Available: https://onlinelibrary.wiley.com/doi/abs/10.1002/pssa.201431744

[13] A. H. Jarndal and G. Kompa, "Large-signal model for AlGaN/GaN HEMTs accurately predicts trapping- and self-heating-induced dispersion and intermodulation distortion," *IEEE Transactions on Electron Devices*, vol. 54, pp. 2830–2836, 2007. [Online]. Available: https://api.semanticscholar.org/CorpusID:8761200

[14] O. Jardel, R. Sommet, J.-P. Teyssier, and R. Quéré, *Nonlinear characterization and modeling of dispersive effects in high-frequency power transistors*, ser. The Cambridge RF and Microwave Engineering Series. Cambridge University Press, 2011, p. 206–256.

[15] M. Iwamoto, J. Xu, and D. E. Root, *DC and thermal modeling: III–V FETs and HBTs*, ser. The Cambridge RF and Microwave Engineering Series. Cambridge University Press, 2011, p. 18–42.

[16] H. Statz, P. Newman, I. Smith, R. Pucel, and H. Haus, "GaAs FET device and circuit simulation in SPICE," *IEEE Transactions on Electron Devices*, vol. 34, no. 2, pp. 160–169, 1987.

[17] W. Curtice, "A MESFET model for use in the design of GaAs integrated circuits," *IEEE Transactions on Microwave Theory and Techniques*, vol. 28, no. 5, pp. 448–456, 1980.

[18] I. Angelov, H. Zirath, and N. Rosman, "A new empirical nonlinear model for HEMT and MESFET devices," *IEEE Transactions on Microwave Theory and Techniques*, vol. 40, no. 12, pp. 2258–2266, 1992.

[19] A. Materka and T. Kacprzak, "Computer calculation of large-signal GaAs FET amplifier characteristics," *IEEE Transactions on Microwave Theory and Techniques*, vol. 33, no. 2, pp. 129–135, 1985.

[20] G. Crupi, V. Vadalà, P. Colantonio, E. Cipriani, A. Caddemi, G. Vannini, and D. M. M.-P. Schreurs, "Empowering GaN HEMT models: The gateway for power amplifier design," *International Journal of Numerical Modelling: Electronic Networks, Devices and Fields*, vol. 30, no. 1, p. e2125, 2017, e2125 JNM-15-0102.R1. [Online]. Available: https://onlinelibrary.wiley.com/doi/abs/10.1002/jnm.2125

[21] S. R. Nedeljkovic, W. J. Clausen, F. Kharabi, J. R. McMacken, and J. M. Gering, *Extrinsic parameter and parasitic elements in III–V HBT and HEMT modeling*, ser. The Cambridge RF and Microwave Engineering Series. Cambridge University Press, 2011, p. 43–85.

[22] D. E. Root, J. Xu, J. Horn, and M. Iwamoto, *The large-signal model: theoretical foundations, practical considerations, and recent trends*, ser. The Cambridge RF and Microwave Engineering Series. Cambridge University Press, 2011, p. 123–170.

[23] C. Wang, Y. Xu, X. Yu, C. Ren, Z. Wang, H. Lu, T. Chen, B. Zhang, and R. Xu, "An electrothermal model for empirical large- signal modeling of AlGaN/GaN HEMTs including self-heating and ambient temperature effects," *IEEE Transactions on Microwave Theory and Techniques*, vol. 62, no. 12, pp. 2878–2887, 2014.

[24] P. Luo, F. Schnieder, O. Bengtsson, V. Vadalà, A. Raffo, W. Heinrich, and M. Rudolph, "A streamlined drain-lag model for GaN HEMTs based on pulsed s-parameter measurements," *International Journal of Microwave and Wireless Technologies*, vol. 11, no. 2, p. 121–129, 2019.

[25] I. Angelov, L. Bengtsson, and M. Garcia, "Extensions of the Chalmers nonlinear HEMT and MESFET model," *IEEE Transactions on Microwave Theory and Techniques*, vol. 44, no. 10, pp. 1664–1674, 1996.

[26] P. Luo, F. Schnieder, and M. Rudolph, "Chalmers GaN HEMT charge model revisited," in *2018 11th German Microwave Conference (GeMiC)*, 2018, pp. 164–167.

[27] L. Liu, "An improved nonlinear model of HEMTs with independent transconductance tail-off fitting," *Journal of Semiconductors*, vol. 32, no. 2, p. 024004, feb 2011. [Online]. Available: https://dx.doi.org/10.1088/1674-4926/32/2/024004

[28] M. L. Hergt, "Characterisierung und Modellierung von Leistungshalbleitern im Frequenzbereich," Doctoral thesis, Karlsruhe Institute of Technology, Karlsruhe, Germany, June 2021.

[29] M. Hergt, L. W. Mayer, M. Sack, M. Honsberg, S. Nielebock, and M. Hiller, "Characterization of parasitic elements in capacitors for fast-switching resonant converters," in *IECON 2019 - 45th Annual Conference of the IEEE Industrial Electronics Society*, vol. 1, 2019, pp. 4095–4100.

[30] M. Hergt, B. Hammer, L. W. Mayer, M. Sack, M. Honsberg, S. Nielebock, and M. Hiller, "Modelling and characterization of power semiconductors in the frequency domain," in *2024 Energy Conversion Congress and Expo Europe (ECCE Europe)*, 2024, pp. 1–8.

[31] A. Jarndal and G. Kompa, "An accurate small-signal model for AlGaN-GaN HEMT suitable for scalable large-signal model construction," *IEEE Microwave and Wireless Components Letters*, vol. 16, no. 6, pp. 333–335, 2006.

[32] F. Lin, "Ein Verfahren zur zuverlässigen experimentellen Modellierung von Mikrowellen-FETs," Doctoral thesis, University of Kassel, Kassel, Germany, 1993.

[33] I. Angelov, K. Andersson, D. Schreurs, D. Xiao, N. Rorsman, V. Desmaris, M. Sudow, and H. Zirath, "Large-signal modelling and comparison of AlGaN/GaN HEMTs and SiC MESFETs," in *2006 Asia-Pacific Microwave Conference*, 2006, pp. 279–282.

[34] A. Parker and J. Rathmell, "Broad-band characterization of fet self-heating," *IEEE Transactions on Microwave Theory and Techniques*, vol. 53, no. 7, pp. 2424–2429, 2005.

[35] *Modeling the Thermal Behavior of GaNPX and PDFN packages Using RC Thermal SPICE Models*, GaN Systems, 03 2022. [Online]. Available: https://gansystems.com/design-center/application-notes/

[36] *GS66504B. Bottom-side cooled 650 V E-mode GaN transistor*, GaN Systems, 2020, rev 200402. [Online]. Available: https://gansystems.com/gan-transistors/gs66504b/

[37] *Curve fitting toolbox*, The MathWorks Inc., Natick, Massachusetts, United States, 2024. [Online]. Available: https://www.mathworks.com/help/curvefit/index.html